ADVANCED FUNCTIONAL MATERIALS
www.afm-journal.de

Liquid Crystal Enabled Early Stage Detection of Beta Amyloid Formation on Lipid Monolayers

*Monirosadat Sadati, Aslin Izmitli Apik, Julio C. Armas-Perez, Jose Martinez-Gonzalez, Juan P. Hernandez-Ortiz, Nicholas L. Abbott, and Juan J. de Pablo**

Liquid crystals (LCs) can serve as sensitive reporters of interfacial events, and this property has been used for sensing of synthetic or biological toxins. Here it is demonstrated that LCs can distinguish distinct molecular motifs and exhibit a specific response to beta-sheet structures. That property is used to detect the formation of highly toxic protofibrils involved in neurodegenerative diseases, where it is crucial to develop methods that probe the early-stage aggregation of amyloidogenic peptides in the vicinity of biological membranes. In the proposed method, the amyloid fibrils formed at the lipid–decorated LC interface can change the orientation of LCs and form elongated and branched structures that are amplified by the mesogenic medium; however, nonamyloidogenic peptides form ellipsoidal domains of tilted LCs. Moreover, a theoretical and computational analysis is used to reveal the underlying structure of the LC, thereby providing a detailed molecular-level view of the interactions and mechanisms responsible for such motifs. The corresponding signatures can be detected at nanomolar concentrations of peptide by polarized light microscopy and much earlier than the ones that can be identified by fluorescence-based techniques. As such, it offers the potential for early diagnoses of neurodegenerative diseases and for facile testing of inhibitors of amyloid formation.

1. Introduction

A wide variety of neurodegenerative diseases such as Alzheimer's and Huntington's, as well as localized diseases such as type-II diabetes, are linked to the aggregation of proteins into amyloid fibrils.[1] Several lines of evidences suggest that the amyloid fiber formations in these diseases are lipid membrane-associated processes and lipids can speed up the aggregation process by orders of magnitude.[2] Although larger aggregates are clinically relevant, small ones are more important because of their potential toxicity and their key role in the onset of disease.[3] It is therefore essential to design a method to probe the protein aggregation process, particularly at early stages and in the vicinity of biological membranes, where much of the aggregations are thought to occur.

Methods capable of probing the formation of amyloid fibrils in inhomogeneous environments, including interfaces or biological membranes, could help accelerate the study of peptide–lipid interactions and could facilitate the screening of amyloid fibril formation inhibitors. Existing approaches for detection of fibril formation rely on Langmuir monolayers, lipid vesicles and supported bilayers.[2b,4]

Recent studies of peptide–lipid interactions by using glazing incidence X-ray diffraction and X-ray and neutron specular reflectivity have confirmed the conformational changes and the aggregation of amyloid beta peptide 1–40 (Aβ) and human islet amyloid polypeptide (hIAPP) in the presence of negatively charged lipid monolayers.[5] Although these characterization techniques are highly precise, they are time consuming and expensive.

Moreover, amyloid fibrils can be directly observed by utilizing fluorescence microscopy with fluorescent dyes such as Thioflavin T (ThT) and Congo red. In particular, ThT is highly selective for amyloid fibrils. When bound to the aggregates, it exhibits a bright fluorescence emission at ≈482 nm but has a low emission in the presence of native proteins comprising different secondary structures.[6] Dye binding and fluorescence are useful indeed for detection of large aggregates; however, they are not particularly effective for detection of the early-stage oligomers[7] that are believed to play a key role in the disease progression.[8] Another disadvantage of fluorescence-based methods is that exogenous compounds, such as quercetin, curcumin, or resveratrol, can bias ThT fluorescence.[9]

Dr. M. Sadati, Dr. J. C. Armas-Perez,
Dr. J. Martinez-Gonzalez, Prof. J. P. Hernandez-Ortiz,
Prof. J. J. de Pablo
Institute for Molecular Engineering
University of Chicago
Chicago, IL 60637, USA
E-mail: depablo@uchicago.edu
Dr. A. I. Apik, Prof. N. L. Abbott
Chemical and Biological Engineering
University of Wisconsin
Madison, WI 53706, USA
Prof. J. P. Hernandez-Ortiz
Departamento de Materiales y Minerales
Facultad de Minas, Universidad Nacional de Colombia
Sede Medellín, Calle 75 # 79A-51
Bloque M17, Medellín, Colombia
Prof. J. J. de Pablo
Argonne National Laboratory
Argonne, IL 60439, USA

DOI: 10.1002/adfm.201502830

Liquid crystals (LCs) have shown to be faithful reporters of binding events at interfaces. The optical properties of a liquid crystal are particularly sensitive to its orientation at an interface. Individual events that disrupt such orientation, including the adsorption of a molecule, lead to a macroscopic reorganization of the liquid crystal that can be detected by simple optical methods. In fact, the liquid crystal acts as an amplifier for molecular binding events.[10] Note, however, that past research in this area has been limited to reporting the adsorption of biomaterials at LC interfaces, including biological toxin,[11] proteins,[12] and stem cells.[13] In this work we go beyond that, and demonstrate that LCs can serve as faithful reporters of distinct molecular motifs, such as the alpha helices or beta sheets of protein aggregates. Specifically, we demonstrate that protofibrils imprint their structure into a liquid crystal interface, and that such a structure propagates into the LC over distances that in some cases approach 20 μm. Our experiments are accompanied by an advanced theoretical and computational analysis of the LC, which provides a detailed view of the local structure of the material as a function of position and proximity to the peptide interface.

To do so, we examine the aggregation of six polypeptides and proteins at a lipid monolayer at an aqueous–liquid crystal interface. The polypeptides include Aβ, which is involved in Alzheimer's disease, hIAPP, which is associated with type-II diabetes, and a polyglutamine chain consisting of 16 glutamine residues, polyglutamine peptide with sequence K2Q16K2 (Q16). Polyglutamine has been implicated in Huntington's disease. All of these molecules are known to aggregate in aqueous solution and form β-sheet structures and amyloid fibrils.[2a,14] We also examine the behavior of three nonaggregating peptides, including rat islet amyloid polypeptide, rIAPP (which represents a small variation of hIAPP), ovispirin and bovine serum albumin, BSA.

2. Results and Discussion

All the experiments in this work were performed at 25 °C, at which the liquid crystal, 4′-pentyl-4-cyanobiphenyl (5CB) is in its nematic phase. We used a lipid monolayer of 1-palmitoyl-2-oleoly-sn-glycero-3-phosphocholine (POPC):1-palmitoyl-2-oleoyl-sn-glycero-3-phospho-(1′-rac-glycerol) (sodium salt) (POPG) 3:1 mixture and a subphase of phosphate–buffer saline (PBS) buffer with pH 7.4. These lipid and subphase conditions were chosen because they are representative of biological membrane systems.[15]

The lipid monolayer with a controlled areal density was transferred onto the LC films using Langmuir–Schaefer transfer (**Figure 1**a–d). The controlled molecular areal density of 66 Å^2 per molecule was obtained by compressing the lipid solution that was originally spread on the surface of (PBS) (Figure 1e). At this areal density, when the lipid monolayer is transferred to the LC–aqueous interface, a homeotropic (or perpendicular) orientation of the LC is observed under polarized light. Therefore, the 5CB filled gold grids appear uniformly dark, with bright edges that are caused by the interaction of the LC with the vertical walls of the gold grid (Figure 1f). Similar observations have

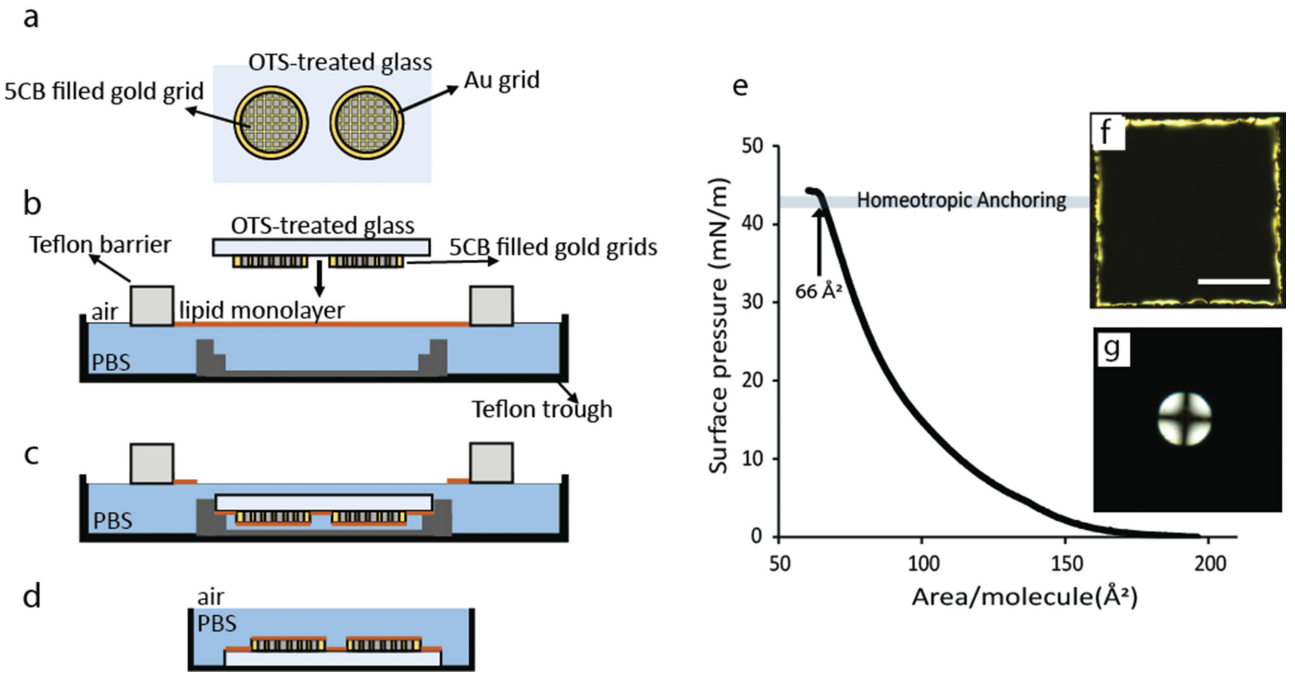

Figure 1. Schematic illustration of the experimental set up used to transfer the Langmuir lipid monolayer at prescribed surface density from air–PBS interface onto an aqueous–LC interface. a) 5CB LC is confined inside transmission electron microscopy (TEM) gold grids supported on a glass slide treated with octadecyltrichlorosilane (OTS). OTS treated glass induces homeotropic alignment of LCs. b) POPC:POPG 3:1 lipid monolayer is compressed to the areal density of 66 Å^2 per molecule (the surface pressure–area isotherm of POPC:POPG 3:1 monolayer measured on PBS subphase at 25 °C is shown in Figure 1e). c) The lipid monolayer is transferred on the aqueous–LC interface. d) The sample is transferred to a PBS cell for further examination. f) Polarized light image and g) the corresponding conoscope image confirm a uniform homeotropic alignment of the LCs after transferring the lipid monolayer. The scale bar is 100 μm.

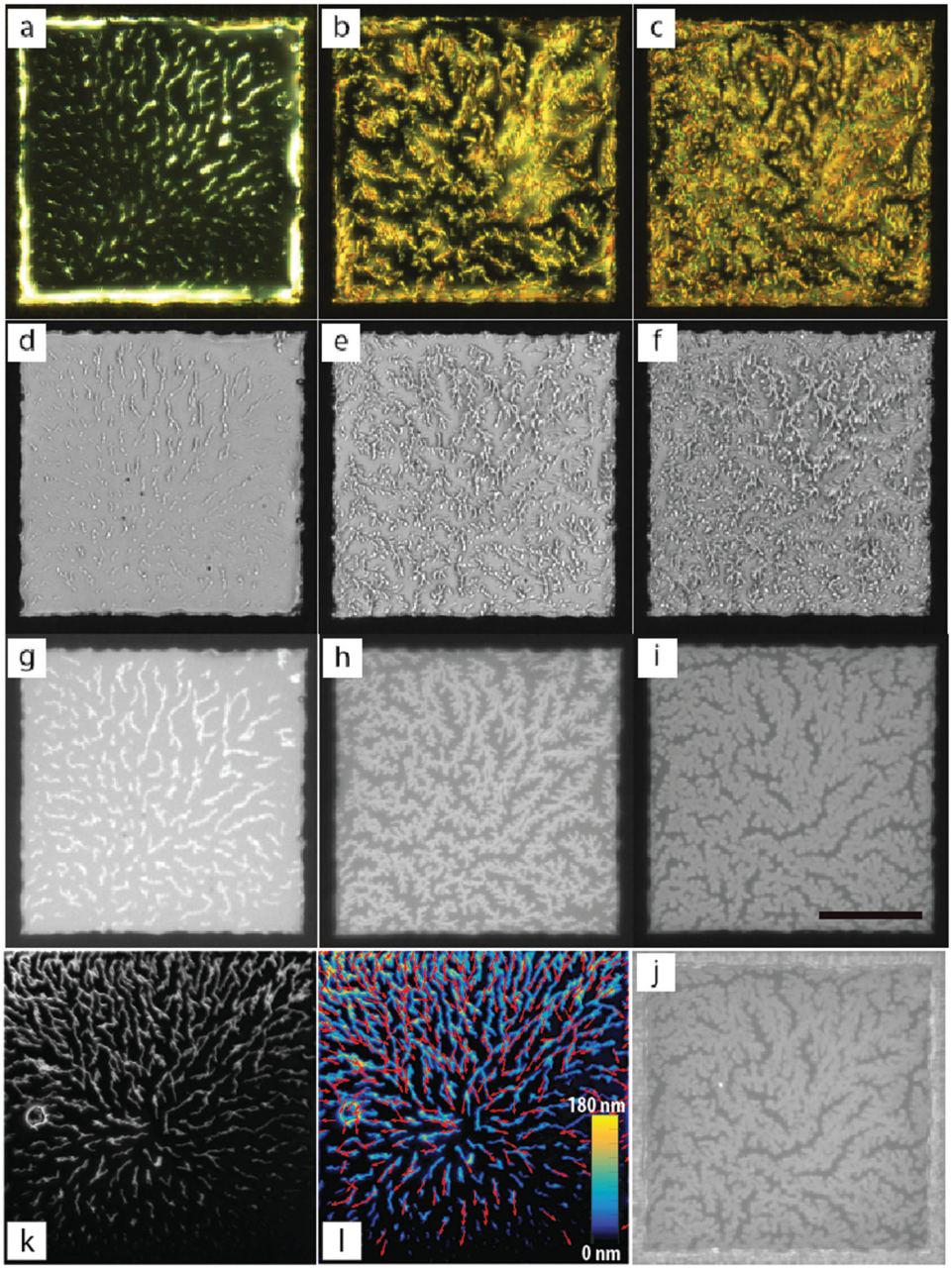

Figure 2. Dynamic optical response of the lipid-laden interface of LC to Aβ adsorption. a–c) Polarized light images, d–f) images obtained by removal of the analyzer, and g–i) epifluorescence images of Texas Red-labeled Aβ. j) The epifluorescence image of ThT fluorescence at the end of the experiment. The images are taken at a,d,g) 5 min, b,e,h) 30 min, c,f,i,j) and 1 h and 30 min after the injection of the peptide into the aqueous phase. Panels (k,l) are phase contrast and liquid crystals retardation map, respectively, which are measured on a different sample. Vectors in panel (l) represent the orientation of the liquid crystals. The scale bar is 100 μm.

been reported elsewhere for Langmuir–Schaefer transfer of L-α-dilauroylphosphatidylcholine[16] and monosialoganglioside GalBeta1-3GalNAcBeta1-4(NauAcAlpha2-3)GalBeta1-4GlcBeta1-1′-Ceramide.[17] Past studies have concluded that the density of the amphiphilic molecules at the interface plays a key role in determining the orientation of the liquid crystal with which they are in contact.[11,16,17]

Previous studies have also shown that the Aβ peptide inserts into negatively charged lipid monolayers.[2b,5a,18] To monitor the interaction between Aβ and the negatively charged lipid monolayer in our hybrid liquid crystal system, we added Aβ into the PBS subphase to reach the total peptide concentration of 250 nM in contact with the lipid–decorated liquid crystal interface.

Approximately 2 min after the addition of the peptide, linear, branch-like structures began to develop throughout the liquid crystal image viewed under polarized light (**Figure 2**a). These patterns were also visible when the analyzer was removed (Figure 2d).

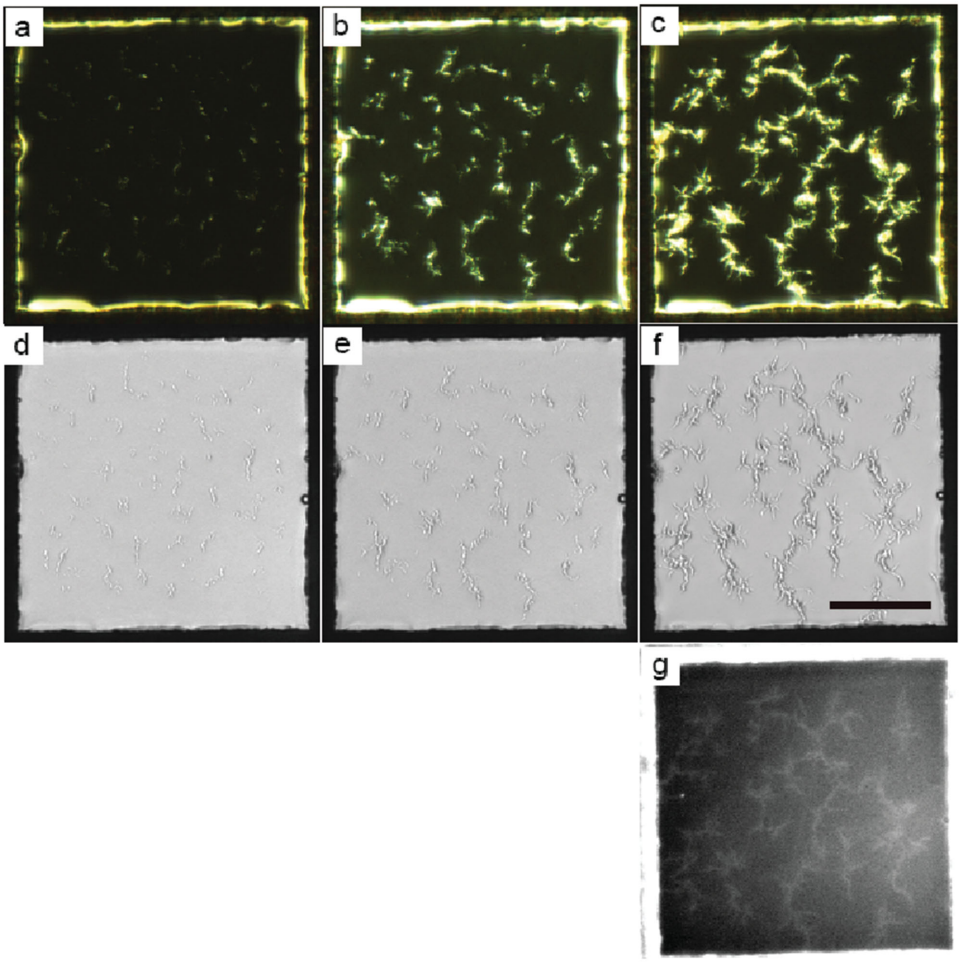

Figure 3. Dynamic optical response of the lipid-laden interface of LC to hIAPP adsorption. a–c) Polarized light images and d–f) images obtained by removal of the analyzer. g) The epifluorescence image of ThT fluorescence at the end of the experiment. This image was digitally enhanced to accentuate the fluorescent regions. The images are taken at a,d) 3 h, b,e) 6 h, and c,f,g) 18 h after injection of the peptide into the aqueous phase. The scale bar is 100 μm.

In order to confirm that these domains correspond to regions where the peptide interacts with the lipid monolayer on the liquid crystal film, we used Texas Red-labeled Aβ, TR-Aβ, and analyzed the sample with epifluorescence microscopy (Figure 2g). The bright domains of the fluorescently labeled Aβ viewed through the epifluorescence microscope correspond to the bright domains of liquid crystal observed under polarized light.

These domains continued to grow and branch out until equilibrium was attained after ≈1 h (Figure 2c). At this point, we performed a thioflavin-T (ThT) binding assay, which is commonly used to identify the presence of beta-amyloid fibrils. The dye thioflavin-T was added to the subphase to reach a 5 μM concentration in the aqueous phase and allowed to bind to the peptide for 15 min. The equilibrium structures observed under polarized light (Figure 2c), after removing the analyzer (Figure 2f) and employing epifluorescence microscopy with the Texas Red filter (Figure 2i), correspond to structures observed under epifluorescence microscopy with the ThT filter (Figure 2j). Increased ThT fluorescence indicates that the branched structures formed by the liquid crystals correspond to peptide aggregates arranged into β-sheet structures.

A second, particularly intriguing molecular system with which to investigate the optical response of the liquid crystal to β-sheet formation and aggregation is provided by the 37-residue islet amyloid polypeptide. The human version of this peptide, hIAPP, forms amyloid deposits in the extracellular regions of the islet β cells of patients with type II diabetes. It is believed that hIAPP fibrils and the oligomers in the aggregation process damage the β cell membrane, resulting in cell death.[19] The hIAPP peptide is interesting in the context of this work because, as an important analog of hIAPP, the rat variant of islet amyloid polypeptide (rIAPP) does not form fibrils. Although rIAPP differs from the human version only at six residues, it does not form β-sheet structures or aggregates.[14c,20] Once hIAPP was added into the aqueous phase, elongated and branched domains similar to those observed with Aβ were formed (**Figure 3**). Over time, these structures merged together and gradually increased in size. The ThT fluorescence confirmed that the domains revealed by the liquid crystals correspond to the β-sheet peptide aggregates at the interface (Figure 3g).

However, when the experiment was repeated with the nonamyloidogenic rIAPP, rounded domains corresponding to a

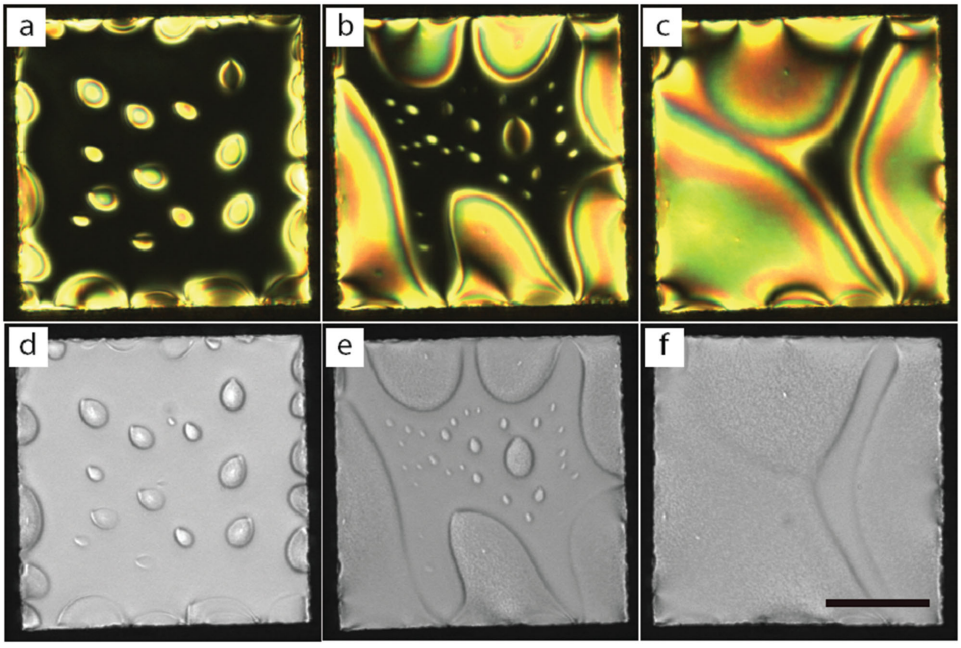

Figure 4. Dynamic optical response of the lipid-laden interface of LC to rIAPP adsorption. a–c) Polarized light images and d–f) images obtained by removal of the analyzer. The images are taken at a,d) 2 h, b,e) 4 h, and c,f) 6 h after the addition of the peptide into the aqueous phase. The scale bar is 100 μm.

tilted orientation of the LC were formed that merged together over time (**Figure 4**). ThT fluorescence could not be detected, which confirms the absence of aggregation and amyloid fibril formation in this system. In agreement with the ThT results, the circular dichroism (CD) spectroscopy measurement in POPC:POPG 3:1 vesicle solution revealed that hIAPP primarily adapts β-sheet structure (76%). β-sheet structure is characterized by the negative CD band around 215 nm. In contrast, rIAPP adopts a completely α-helical conformation, which is evidenced by two negative CD bands at 222 and 208 nm (Figure S1, Supporting Information).

To further substantiate our findings, we also considered polyglutamine chains of 16 residues. It has been shown that polyglutamine chains of 16 residues, "Q16," form aggregates in PBS solution.[21] We studied the peptide sequence $K_2Q_{16}K_2$, where the lysines were added to the ends of the molecule in order to increase its solubility in water. To eliminate the charge interactions of the termini, the N terminus was acetylated and the C terminus was amidated.[21] Surprisingly, elongated and branched domains were formed (**Figure 5**a) only 2 h after adding Q16 into the aqueous subphase on the lipid decorated LC. The ThT fluorescence assay confirmed that these domains correspond to the β-sheet formation and peptide aggregates at the interface (Figure 5g).

However, similar to the hIAPP peptide, the ThT experiment on Q16 was only able to detect the β-sheet secondary structure long after the liquid crystals did (after about 26 h). Although it is useful for detection of large aggregates, the ThT dye binding is not particularly effective for detecting the early-stage oligomers that are presumed to play an important role in the onset of amyloid diseases.[8]

As negative controls, we also examined the behavior of a large, nonamyloidogenic protein, namely BSA and the 18-residue ovispirin. The 18-residue ovispirin antimicrobial peptide adopts an α-helical conformation in the bulk and in the vicinity of lipids.[22] When these peptides were added into the aqueous phase on the lipid decorated liquid crystal interface, they did not form any branched domains, but instead adopted the appearance of rounded domains that merged together over time (**Figure 6** and Figure S2, Supporting Information). Neither BSA nor ovispirin formed amyloid fibrils, and the addition of ThT did not result in fluorescence. Using fluorescently labeled BSA and lipids, de Tercero and Abbott[23] were able to show that the bright domains in the LC image under polarized light correspond to regions where peptide fluorescence is observed, while dark domains correspond to lipid-rich regions.

All of the amyloid fibril forming peptides considered in this study (Aβ, hIAPP, and Q16) led to formation of elongated, branched structures whose β-sheet character was confirmed by the ThT fluorescence and circular dichorism measurements. As mentioned earlier, protein adsorption at lipid decorated LC–aqueous interfaces has been examined before in a different context for mouse IgG_1, goat IgG, NeutrAvidin, and phospholipase A_2 (PLA_2).[10a,12b,23] What was not recognized in these past studies, however, was that all of these peptides are rich in β-sheet structure and interact with lipid membranes. The secondary structure of IgG consists mainly (76%) of β-sheets and the α-helical content is small.[24] Fourier transform infrared spectroscopy (FTIR) studies have shown that Avidin consists of 66% β-sheet secondary structure; the remainder of the molecule consists of β-turns and unstructured peptide.[25] Avidin has been shown to interact with negatively charged lipids and to form peptide-lipid assemblies.[25] PLA_2 forms amyloid fibrils and causes an increase in ThT fluorescence.[26] Fibrillar structures of PLA_2 have been observed by atomic force microscopy

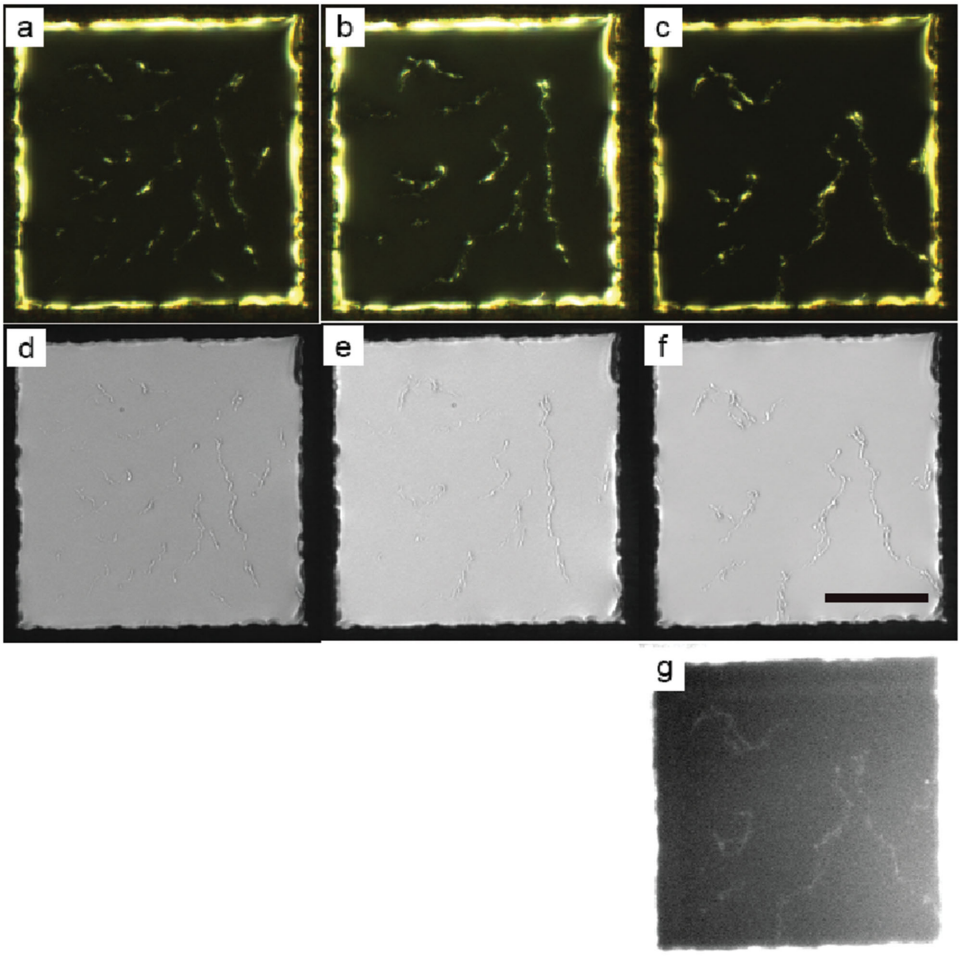

Figure 5. Dynamic optical response of the lipid-laden interface of LC to Q16 adsorption. a–c) Polarized light images and d–f) images obtained by removal of the analyzer. g) The epifluorescence image of ThT fluorescence at the end of the experiment. This image was digitally enhanced to accentuate the fluorescent regions. The images are taken at a,d) 2 h, b,e) 8 h, and c,f,g) 26 h after the addition of the peptide into the aqueous phase. The scale bar is 100 μm.

and by electron microscopy in the presence of dipalmitoylphosphatidylcholine (DPPC) bilayers.[26] Indeed, when reexamined on a liquid crystal, these three proteins—IgG, Avidin, and PLA_2—form elongated, branched structures analogous to those reported here.

In contrast, all the nonamyloidogenic peptides considered here (rIAPP, BSA, and ovispirin) resulted in tilted liquid crystal domains and did not induce ThT fluorescence. At equilibrium, those circular domains grow and merge together until liquid crystals, all over the grid, adopt a tilted orientation. Previous studies have also revealed comparable arrangements with cytochrome C,[23] which is almost entirely α-helical.[27]

In fact, the density of the amphiphilic molecules at the interface plays a key role in determining the orientation of the liquid crystal with which they are in contact.[11,16,17] When lipid monolayers at low lipid densities are transferred to the aqueous–LC interface, a tilted orientation is observed.[16] It has been shown that upon adsorption of protein molecules at the lipid-laden LC interface, they can penetrate into the lipid monolayer and consequently change the local areal density of the lipid molecules. The selective ordering transition of the liquid crystals to the protein structure can therefore be considered as a direct indication of competitive interactions of lipid monolayer and peptides with the liquid crystals.

De Tercero and Abbott[23] argued that the bright ellipsoidal domains observed with BSA or cytochrome C may be caused by the stronger protein–protein interaction compared to the lipid–protein interaction. The proteins try to minimize the lipid–protein interaction and maximize the protein–protein interaction, which may lead to the separated domains for the lipid and protein (Figures 4 and 6). By contrast, peptides that form branched structures exhibit strong protein–lipid interactions. They are all peptides that are known to interact with lipids, thereby resulting in aggregation and membrane cytotoxicity. We speculate that such peptides can be incorporated into the lipid monolayer instead of pushing it away.

Regardless of their specific sequence, all these disease-causing peptides exhibit fibrillar amyloid structures and directional ordering. Mapping the local optical retardation and orientation of the liquid crystals using the quantitative birefringence imaging technique, PolScope,[28] proves that in spite of the local ordering of the liquid crystals in the presence of

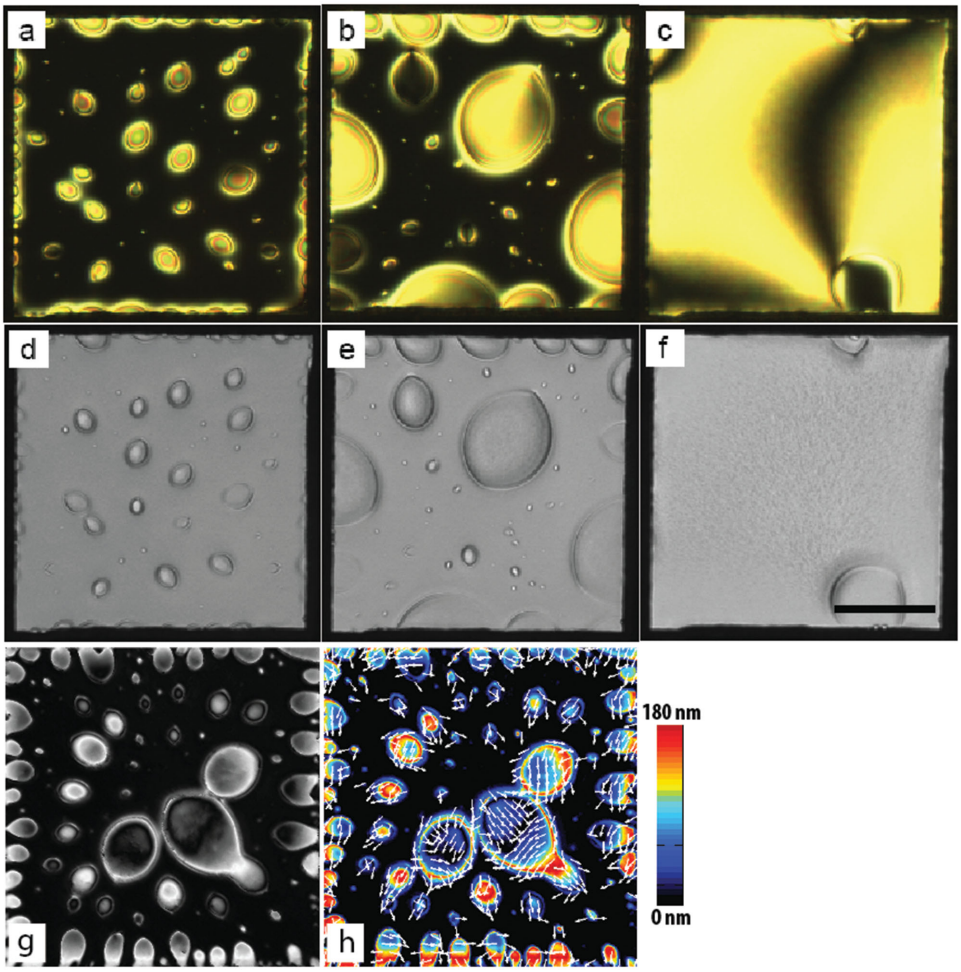

Figure 6. Dynamic optical response of the lipid-laden interface of LC to BSA adsorption. a–c) Polarized light images and d–f) images obtained by removal of the analyzer. The images are taken at a,d) 20 min, b,e) 1 h, and c,f) 14 h after the addition of the peptide into the aqueous phase. g,h) Phase contrast and liquid crystals retardation map, respectively, which are measured on a different sample. Vectors in panel (h) represent the orientation of the liquid crystals. The scale bar is 100 μm.

BSA (Figure 6h), they are predominantly aligned along the fibrils when exposed to a β-sheet forming peptide (Figure 2l). The ordered structure in amyloidogenic peptides prevents them from spreading uniformly on the mobile monolayer at the aqueous–LC interface, and instead they form networks of peptide fibrils. These networks give rise to an elongated and branched appearance of the liquid crystals under polarized light, which can be regarded as a signature of amyloid-forming peptides.

Up to this point, our discussion of amyloid-fibril induced branched morphologies has focused on qualitative experimental observations. In fact, much of the literature on molecular adsorption at LC interphases has relied almost exclusively on experimental information. Some of the central questions that arise, however, are (i) to what extent is the orientation of the underlying LC altered by the presence of β-rich amyloid fibrils? (ii) is that orientation any different when unstructured or α-helical aggregates are deposited at the interface, and (iii) how strong is the anchoring of the LC at the peptide? To address these issues, we rely on a Landau-de Gennes free energy description of the LC and the interface and explore the LC morphology that arises at equilibrium. The free energy functional (or Hamiltonian) is constructed with a biaxial **Q**-tensor representation that includes short-range contributions to the energy (which control the isotropic–nematic transition), long-range contributions to the free energy to account for twist, bend, and splay elastic deformation modes, and surface contributions to the free energy that control the local LC alignment at the interphases.[29] The free energy functional is denoted by $F = F\left(A,U,k_{11},k_{22},k_{33},W_{\mathrm{H}},W_{\mathrm{P}},Q,\nabla Q\right)$: where U controls the isotropic–nematic transition, A sets the energy scale, k_{11}, k_{22}, and k_{33} are nonvanishing elastic moduli corresponding to independent splay, twist, and bend[30] deformation modes, and W_{H} and W_{P} represent the strength of perpendicular (or homeotropic) and planar anchoring, respectively. For 5CB, the following values from the literature are used in this work: $A \approx 1 \times 10^5$, $k_{11} = k_{33} = 6$ pN and $k_{22} = 3$pN.[29a,31] The isotropic–nematic transition parameter is set to $U = 3.165$, which corresponds to a bulk value of the scalar order parameter of S ≈ 0.54.[31] Additional details pertaining to the model and the simulations are provided in the Supporting Information. Note that the lipid monolayer induces a perpendicular

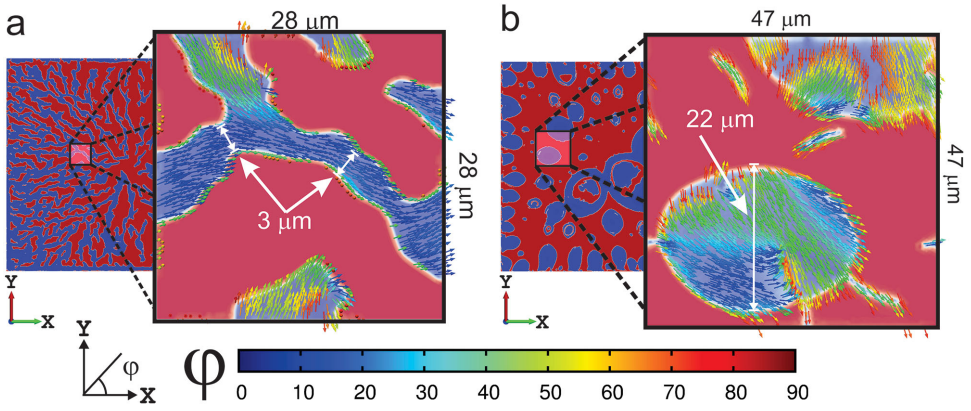

Figure 7. Top view of the LC lipid-laden interface with a) Aβ and b) BSA peptides. Red regions correspond to homeotropic anchoring lipid areas. Blue regions correspond to planar anchoring peptide-rich areas. The local LC orientation is also shown for two small, representative peptide-rich regions, where the color code represents the azimuthal angle of the LC on the XY-plane.

alignment to the LC–aqueous interface with an anchoring strength $W_H = 1 \times 10^{-4}$ J m^{-2}.[32] At the bottom substrate, strong homeotropic anchoring is imposed, with a coefficient $W_H = 1 \times 10^{-2}$ J m^{-2}. As can be appreciated in **Figure 7**, the surface area covered by the peptide induces degenerate planar anchoring of the LC. The anchoring strength for the "peptide area," W_P, is unknown; therefore, a range of strengths between 10^{-2} and 10^{-5} J m^{-2} was considered here until the splay-bend deformation was captured by our simulations.

Figure 7 shows some of the results of our simulations. In the top view of the lipid/protein surfaces, red domains correspond to the homeotropic-anchored lipid-laden region, and blue domains represent the planar-anchored peptide covered areas. According to the PolScope birefringence measurements (Figure 2k), the average width of the branched structure of the Aβ peptide is around 3 μm (Figure 7a). By contrast, BSA rich domains (Figure 6g) expand over larger areas (>10 μm in length, Figure 7b). The experimentally observed interfacial domains were used as input boundary conditions for the relaxation of the underlying LC in simulations. These boundary conditions therefore consist of inhomogeneous parallel and perpendicular domains. In Figure 7, domain sizes are 28 × 28 × 20 μm for Aβ and 47 × 47 × 20 μm for BSA. The LC at the bottom surface experiences strong homeotropic anchoring. Figure 7 also depicts the LC orientation in the peptide-covered areas; the color scheme in the figure corresponds to the azimuthal angle φ on the XY-plane. Note that, for the Aβ peptide, the director of the LC follows closely the direction of the peptide-covered areas. In contrast, one can see that for the BSA peptide multiple domains with different orientations appear under the peptide. The reason for this different response by the LC to a fibril (Aβ) or a disordered aggregate (BSA) has to do with the elastic distortion induced by the combined homeotropic and planar regions. At the boundary between lipid and peptide-rich regions, there is an elastic deformation due to the gradual reorientation of the LC from perpendicular to planar. This deformation may follow a splay or a twist mode. For 5CB, the elastic modulus k_{11} that penalizes splay deformations is two times larger than the twist mode, k_{22}. The LC therefore prefers to twist, thereby aligning itself along the direction of the lipid/peptide boundary. This phenomenon sets a "preferred" alignment for the planar domains, which persists over the peptide domain and over length scales that exceed several micrometers (≈3 μm for Aβ, Figure 7a). For circular peptide domains, as the characteristic area increases, the peptide cannot impose a single orientation on the surface, and a multidomain texture arises (Figure 7b for BSA). The larger, more rounded peptide domain has a smaller perimeter and exhibits a weaker boundary effect.

Figure 8 shows a 3D cross section of the simulated domains, illustrating the behavior of the LC between the two surfaces. The strong homeotropic anchoring at the bottom surface forces the LC to adopt a perpendicular orientation at the wall; this alignment is conserved until the LC "feels" the homeotropic or planar anchoring at the top surface. Note that in order to adopt any planar orientation at the top, a splay-bend deformation is required. In a hybrid cell, where one surface is homeotropic and the other one is planar, the change in orientation (zenithal angle θ in Figure 8) is a linear function of the cell thickness.[33] For hybrid anchoring, the zenithal angle is also a function of the interaction of the LC with the peptide and the lipid, i.e., the relative coverage. To further characterize the system we introduce a scalar value γ, given by the dot product of the local director **n** and a unit vector along the Z-axis, **z**. The isosurface for $\gamma = 0.75$ is shown in Figure 8 for both, Aβ and BSA. Note that the realignment depth for the Aβ peptide (≈8 μm) is larger than for the BSA peptide (≈3 μm). On the one hand, this may be explained based on the basis that Aβ induces a stronger anchoring than BSA. The simulated anchoring strengths that are better able to describe the PolScope experimental results are $W_P \approx 1 \times 10^{-3}$ J m^{-2} for Aβ and $W_P \approx 1 \times 10^{-4}$ J m^{-2} for BSA; these values are consistent with the hypothesis that anchoring is approximately ten times stronger along the Aβ β-sheets than along the BSA disordered aggregate structure. An additional argument, based on the preferential alignments at the surface, should also be used to further explain the results shown in Figure 8. Recall that, for Aβ, there is a twist deformation at the lipid/peptide boundary and a single alignment along the peptide-covered area (Figure 8a). This alignment propagates through the bulk of the LC cell (Figure 8a), thereby minimizing any elastic penalties that may arise between the undistorted and the splay-bend regions of the material. Through this mechanism, Aβ has a deeper influence (8 μm, as shown in the figure)

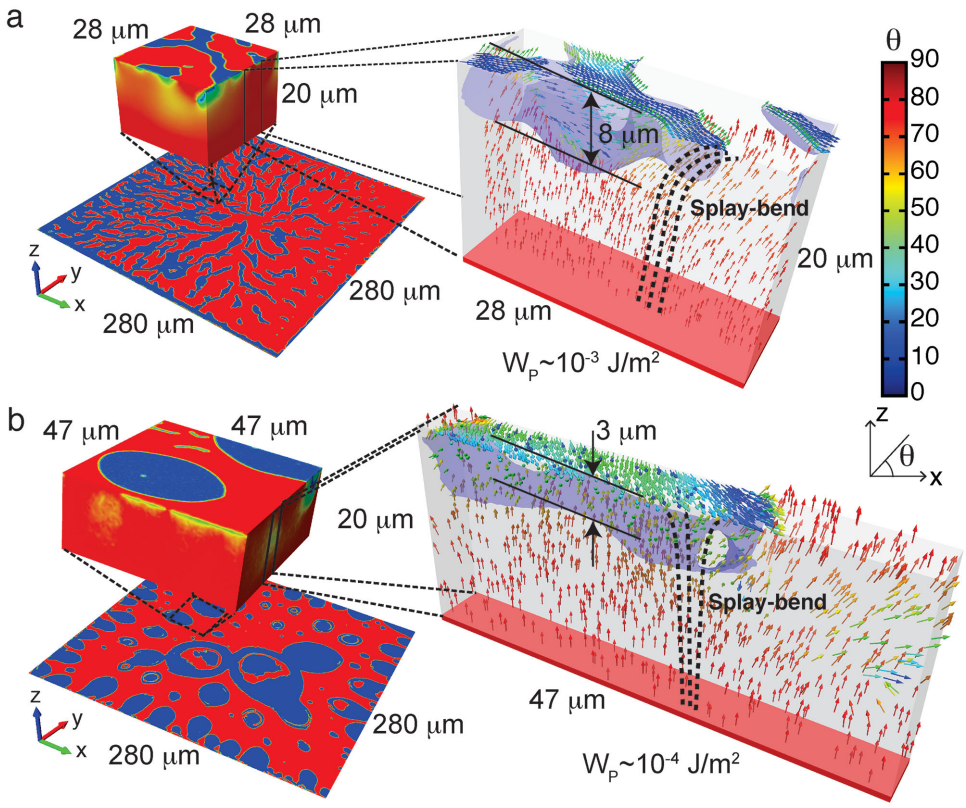

Figure 8. 3D view and representative thin, cross-sectional slices of the simulated domain for a) Aβ and b) BSA. At the top surface, red regions correspond to homeotropic-anchoring lipid-covered areas. Blue regions correspond to planar-anchoring peptide-covered areas. The combination of mixed homeotropic and planar alignment on the top surface and the strong homeotropic anchoring on the bottom surface induces a splay-bend deformation of the LC in the bulk of the films. The LC orientations are included in the 3D slices, where the colors represent the zenithal angle θ, and the arrows show the local director. Near the bottom surface, a perpendicular, undistorted nematic LC phase can be observed. As the LC approaches the top surface, splay-bend distortions accommodate allow the LC orientation to follow the anchoring dictated by the peptide. Isosurfaces of $\gamma = \mathbf{n}\cdot\mathbf{z} = 0.75$, where **n** is the local director vector and **z** is a unit vector along the Z-axis, are included to quantify the peptides' range of influence.

on the LC structure. For BSA, the multidomain texture at the surface induces splay-bend as well as other types of elastic deformations. To minimize such deformations, the system simply reduces the volume over which the parallel/planar transition occurs, thereby leading to thin (3 μm) distorted domains in the immediate vicinity of the peptide.

3. Conclusions

Liquid crystalline materials exhibit unique responses to peptides that aggregate at membrane interfaces. In this work, we have shown that the aggregation of β-sheet forming peptides into fibrils at lipid–decorated liquid crystal interfaces gives rise to branch-like structures on the liquid crystals. In contrast, peptide aggregates with mainly α-helical character exhibit weak protein–lipid interactions and induce formation of circular domains in the underlying liquid crystals. A theoretical and computational analysis of experimentally observed textures reveals that β-sheet rich amyloid fibrils exhibit a relatively strong anchoring energy, of magnitude 10^{-3} J m^{-2}. The influence of the peptides into the liquid crystal film is felt over length scales of ≈8 μm. By contrast, α-helical rich peptide aggregates exhibit a much weaker anchoring energy, ≈10^{-4} J m^{-2}, and the characteristic length scale over which their influence is felt is smaller, in the range of 3 μm. We are not aware of previous works that may have directly examined the range of influence of biological molecules at LC interfaces, and it is therefore difficult to place these magnitudes in the context of past studies. With that caveat, however, it is remarkable that a molecularly thin amyloidogenic peptide layer at an interface induces a disturbance that is in fact amplified by a liquid crystal over length scales approaching ten of micrometers.

These differences in the response of a liquid crystal to fibrils or disordered aggregates could serve as the basis for a possible amyloid-sensing mechanism. In contrast to recently developed techniques for amyloid formation detection based on neuroimaging[34] and biochemical markers,[35] the structural signatures that peptide aggregates impart on liquid crystals could provide the foundation for alternative methods that rely on simple polarized light microscopy, without the need for complicated instrumentation or molecular labels. Most importantly, β-sheet formation can be detected at very early stages, and only nanomolar concentrations of peptide are required. The detection method could also be suitable for developing assays, where different fragments of a cytotoxic peptide or molecules that interfere with aggregation and cytotoxicity could be screened. These results could serve as the basis for sensing devices that

rely on liquid crystal orientation to detect amyloid fibril formation at very early stages in biomedical or clinical settings, where detection by available means has been elusive and where aggregate formation matters the most.

4. Experimental Section

Materials: POPC and POPG were obtained from Avanti Polar Lipids (Alabaster, AL) as 10 mg mL^{-1} solutions in chloroform. Chloroform, hexafluoroisopropanol (HFIP), and BSA were obtained from Sigma-Aldrich (St. Louis, MO); 99.5% trifluoroacetic acid (TFA) for biochemistry was obtained from Acros Organics (Geel, Belgium). Octadecyltrichlorosilane (OTS), PBS, methanol, sulfuric acid, hydrogen peroxide, dichloromethane, and heptane were obtained from Fisher Scientific (Pittsburgh, PA). The LC 4′-pentyl-4-cyanobiphenyl (5CB) was purchased from EM (New York, NY), and Aβ(1–40), TR-Aβ, hIAPP, rIAPP, and ovispirin were all purchased from AnaSpec (Fremont, CA). All chemicals were used without further purification. A polyglutamine peptide with sequence $K_2Q_{16}K_2$ was custom synthesized and high-performance liquid chromatography (HPLC) purified at the UW Biotechnology Center (Madison, WI). Water with a resistivity of 18.2 MΩ cm was obtained by deionizing a distilled water source with a Milli-Q system (Millipore, Bedford, MA). The Finest Premium Grade microscope slides from Fisher Scientific were used for OTS coating, and 20 μm thick, 283 μm grid spaced gold-specimen grids were obtained from Electron Microscopy Sciences (Ford Washington, PA).

Preparation of LC-Filled Grids: Details of the preparation of optical LC-filled grids can be found in our previous publication.[10a,16,23] Briefly, glass slides were cleaned and coated with OTS. The quality of the OTS coating was assessed by sandwiching nematic 5CB between two OTS-treated glass slides. Gold grids were rinsed in ethanol, methanol, and dichloromethane, dried and placed on the surface of a piece of OTS-coated glass slide (Figure 1a). Approximately 1 μL of 5CB was dispensed onto each grid and the excess LC was removed by contacting a 5 μL capillary tube with the 5CB droplet.

Langmuir–Schaefer Transfer of POPC:POPG 3:1 Monolayers on the Aqueous–LC Interface: Previous studies have established that lipid monolayers can be formed at the interface between a thermotropic liquid crystals and an aqueous solution by vesicle fusion[10a,12b] or using Langmuir–Schaefer transfer.[16] Such hybrid systems have been used to study various aspects of protein–lipid interactions.[10a,12] We have chosen here to use Langmuir–Schaefer transfer in order to control the areal density of the lipid monolayer at the interface. Langmuir monolayers were prepared on a Nima 602A film balance (Coventry, England) equipped with a filter paper Wilhelmy plate for surface pressure measurements. The temperature of the trough was kept at 25 °C with a water bath (ISOTEMP 1006D, Fisher Scientific, Pittsburgh, PA). To prepare the Langmuir monolayer, POPC:POPG at a molar ratio of 3:1 and a concentration of 1 mg mL^{-1} was dissolved in chloroform. A known volume of lipid solution was deposited dropwise uniformly across the surface of a PBS buffer with pH = 7.4. The solvent was allowed to evaporate for 20 min before the monolayer compression was initiated at a rate of 100 cm^2 min^{-1}. Once the surface density reached to 66 $Å^2$ per molecule, the 5CB-filled grids supported on an OTS glass slide were inverted, lowered horizontally, passed through the lipid-laden aqueous/air interface using tweezers and placed on a homemade aluminum frame in the bottom of the trough (Figure 1b,c). After the transfer, the glass slide with the grids was removed from the trough and placed in a vial containing PBS for further studies (Figure 1d). A detailed description of the experimental setup for the Langmuir–Schaefer transfer can be found in ref.[16].

Preparation of the Peptide Stock Solutions: Lyophilized powders of Aβ, hIAPP, and rIAPP were dissolved in HFIP at a 1 mg mL^{-1} concentration. The day before using the peptide, HFIP was evaporated in a nitrogen stream and then in vacuum overnight. The peptide film was then dissolved in dimethyl sulfoxide (DMSO) to yield a 1 mg mL^{-1} concentration and the sample was used within 24 h. Ovispirin and BSA were directly dissolved in water at a 1 and a 10 mg mL^{-1} concentration, respectively. Polyglutamine Q16 was dissolved in water to yield a 1 mg mL^{-1} concentration; the pH was adjusted to pH 3 with TFA. Protein stock solutions were added to the aqueous phase, consisting of PBS, to yield peptide concentrations of 250 nM in contact with the POPC:POPG-laden liquid crystal interface.

Epifluorescence Microscopy: The fluorescent images of the Texas Red conjugated Aβ, TR- Aβ, were taken with 1% Texas Red labeled Aβ solution added to the aqueous phase on the POPC:POPG-laden interface with an exposure time of 0.04 s. For the ThT fluorescence images, ThT was added to the system at the end of the experiment to yield a 5 μM final concentration (added from a 5 mM stock solution in deionized water). Note that exceeding the final concentration of 5 μM of the ThT can distort the orientation of liquid crystals. The fluorescent images were taken with an Olympus IX71 inverted microscope equipped with a 100 W mercury lamp and a Hamamatsu 1394 ORCA-ER-CCD camera interfaced to a computer using SimplePCI software. The filters used for ThT and Texas Red were an Olympus U-MNB2 (Center Valley, PA) and a Chroma 41004 (Bellows Falls, VT), respectively. The excitation and emission wavelengths of ThT (450 and 482 nm, respectively) did not overlap with the excitation and emission wavelengths of Texas Red (583 and 603 nm, respectively). The background fluorescence of Texas Red was insignificant when measured with the Olympus filter that was used for ThT fluorescence inspection.

CD Analysis: CD (Jasco J-815 CD Spectrometer) was used to characterize secondary structures of hIAPP and rIAPP. To emulate the experimental condition, the peptides were studied in lipid vesicle solution. To prepare lipid vesicles, 2 mg of lipid mixture (POPC:POPG 3:1) was dissolved in chloroform. The chloroform solvent was evaporated under a stream of nitrogen and further dried under vacuum overnight. The remaining lipid, was then hydrated with PBS buffer (2 mg mL^{-1}), and went through five freeze–thaw cycles. Unilamellar vesicles were achieved by extruding the lipid solution 31 times through a 100 nm pore size polycarbonate membrane (Avanti Polar Lipids, Alabaster, AL). To prepare CD solutions, lyophilized powders of hIAPP and rIAPP were first dissolved in HFIP for 2 h to obtain a 1 mg mL^{-1} peptide solution. HFIP was evaporated under nitrogen stream and then under vacuum overnight. The peptide film was dissolved in PBS buffer to yield a 1 mg mL^{-1} concentration. Stock peptides in PBS were added to vesicle solution to yield mixtures containing 25 μM peptide with 1:20 peptide to lipid mole ratio. Samples were then incubated at 25 °C for 24 h. The circular dichroism spectra were collected between 190 and 250 nm at room temperature in a 1 mm cuvette. Each spectrum is an average of five runs after subtracting the baseline spectrum of buffer and vesicles, without the presence of the peptides. To determine percentages of α-helix, β-sheet, and random coil secondary structures, a linear combination of poly(lysine) basis spectra was fitted on each CD spectrum.[36]

Supporting Information

Supporting Information is available from the Wiley Online Library or from the author.

Acknowledgements

M.S. and A.I.A. contributed equally to this work. The authors are grateful to Dr. Kathleen Cao from the Lee lab at the University of Chicago for her assistance and guidance in running Langmuir Trough experiment. The authors thank Prof. Oleg D. Levrentovich and Young-Ki Kim from the Liquid Crystal Institute of Kent State University for the use of their PolScope instrument. The development of codes and the corresponding calculations and analysis presented in this work were supported by the National Science Foundation, grant DMR-1410674. The original

experimental studies on protein interactions with liquid crystals were supported by the University of Wisconsin MRSEC, grant DMR-1121288. The theoretical and experimental studies of polyglutamine misfolding and aggregation were supported by grant CBET-1264021. The contributions of M.S. were partially supported by the Swiss National Science Foundation (P300P2_151342). J.M.-G. also acknowledges support from CONACYT through Fellowship 250263. The authors declare no competing financial interests.

Received: July 10, 2015
Published online: September 9, 2015

[1] a) I. Benilova, E. Karran, B. De Strooper, *Nat. Neurosci.* **2012**, *15*, 349; b) P. Cao, A. Abedini, H. Wang, L.-H. Tu, X. Zhang, A. M. Schmidt, D. P. Raleigh, *Proc. Natl. Acad. Sci. USA* **2013**, *110*, 19279; c) C. A. Ross, M. A. Poirier, *Nat. Med.* **2004**, *10*, S10.

[2] a) M. Bokvist, F. Lindstrom, A. Watts, G. Grobner, *J. Mol. Biol.* **2004**, *335*, 1039; b) C. Ege, K. Y. C. Lee, *Biophys. J.* **2004**, *87*, 1732; c) S. A. Kotler, P. Walsh, J. R. Brender, A. Ramamoorthy, *Chem. Soc. Rev.* **2014**, *43*, 6692.

[3] a) N. E. Pryor, M. A. Moss, C. N. Hestekin, *Int. J. Mol. Sci.* **2012**, *13*, 3038; b) A. Relini, N. Marano, A. Gliozzi, *Biomolecules* **2013**, *4*, 20.

[4] J. D. Knight, J. A. Hebda, A. D. Miranker, *Biochemistry* **2006**, *45*, 9496.

[5] a) E. Y. Chi, C. Ege, A. Winans, J. Majewski, G. Wu, K. Kjaer, K. Y. C. Lee, *Proteins: Struct., Funct., Bioinfo.* **2008**, *72*, 1; b) S. Kim, D. K. Klimov, *J. Mol. Model.* **2013**, *19*, 737; c) K. Sasahara, K. Morigaki, T. Okazaki, D. Hamada, *Biochemistry* **2012**, *51*, 6908; d) E. Maltseva, A. Kerth, A. Blume, H. Mohwald, G. Brezesinski, *ChemBioChem* **2005**, *6*, 1817.

[6] a) H. Levine, *Protein Sci.* **1993**, *2*, 404; b) M. R. Nilsson, *Methods* **2004**, *34*, 151.

[7] L. A. Munishkina, A. L. Fink, *Biochim. Biophys. Acta, Biomembr.* **2007**, *1768*, 1862.

[8] D. M. Walsh, D. J. Selkoe, *J. Neurochem.* **2007**, *101*, 1172.

[9] S. A. Hudson, H. Ecroyd, T. W. Kee, J. A. Carver, *FEBS J.* **2009**, *276*, 5960.

[10] a) J. M. Brake, N. L. Abbott, *Langmuir* **2007**, *23*, 8497; b) S. I. Hernandez, J. A. Moreno-Razo, A. Ramirez-Hernandez, E. Diaz-Herrera, J. P. Hernandez-Ortiz, J. J. de Pablo, *Soft Matter* **2012**, *8*, 1443; c) Q.-Z. Hu, C-H. Jang, *Liquid Cryst.* **2014**, *41*, 597; d) A. C. McUmber, P. S. Noonan, D. K. Schwartz, *Soft Matter* **2012**, *8*, 4335; e) J. A. Moreno-Razo, E. J. Sambriski, N. L. Abbott, J. P. Hernandez-Ortiz, J. J. de Pablo, *Nature* **2012**, *485*, 86; f) P. Popov, E. K. Mann, A. Jakli, *Phys. Rev. Appl.* **2014**, *1,* 034003; g) V. Tomar, T. F. Roberts, N. L. Abbott, J. P. Hernandez-Ortiz, J. J. de Pablo, *Langmuir* **2012**, *28*, 6124.

[11] I. H. Lin, D. S. Miller, P. J. Bertics, C. J. Murphy, J. J. de Pablo, N. L. Abbott, *Science* **2011**, *332*, 1297.

[12] a) T. Bera, J. Deng, J. Fang, *J. Phys. Chem. B* **2014**, *118*, 4970; b) J. M. Brake, M. K. Daschner, Y. Y. Luk, N. L. Abbott, *Science* **2003**, *302*, 2094; c) D. Hartono, C-Y. Xue, K-L. Yang, L-Y. L. Yung, *Adv. Funct. Mater.* **2009**, *19*, 3574; d) Q-Z. Hu, C-H. Jang, *Analyst* **2012**, *137*, 567; e) J-M. Seo, W. Khan, S-Y. Park, *Soft Matter* **2012**, *8*, 198.

[13] N. A. Lockwood, J. C. Mohr, L. Ji, C. J. Murphy, S. R. Palecek, J. J. de Pablo, N. L. Abbott, *Adv. Funct. Mater.* **2006**, *16*, 618.

[14] a) J. R. Brender, E. L. Lee, M. A. Cavitt, A. Gafni, D. G. Steel, A. Ramamoorthy, *J. Am. Chem. Soc.* **2008**, *130*, 6424; b) L. E. Buchanan, E. B. Dunkelberger, H. Q. Tran, P-N. Cheng, C-C. Chiu, P. Cao, D. P. Raleigh, J. J. de Pablo, J. S. Nowick, M. T. Zanni, *Proc. Natl. Acad. Sci. USA* **2013**, *110*, 19285; c) C. T. Middleton, P. Marek, P. Cao, C-C. Chiu, S. Singh, A. M. Woys, J. J. de Pablo, D. P. Raleigh, M. T. Zanni, *Nat. Chem.* **2012**, *4*, 355; d) S. Singh, C-C. Chiu, A. S. Reddy, J. J. de Pablo, *J. Chem. Phys.* **2013**, *138*,155101; e) L. Wang, C. T. Middleton, S. Singh, A. S. Reddy, A. M. Woys, D. B. Strasfeld, P. Marek, D. P. Raleigh, J. J. de Pablo, M. T. Zanni, J. L. Skinner, *J. Am. Chem. Soc.* **2011**, *133*, 16062.

[15] D. E. Warschawski, A. A. Arnold, M. Beaugrand, A. Gravel, E. Chartrand, I. Marcotte, *Biochim. Biophys. Acta, Biomembr.* **2011**, *1808*, 1957.

[16] M.-V. Meli, I. H. Lin, N. L. Abbott, *J. Am. Chem. Soc.* **2008**, *130*, 4326.

[17] I. H. Lin, M.-V. Meli, N. L. Abbott, *J. Colloid Interface Sci.* **2009**, *336*, 90.

[18] A. Izmitli, C. Schebor, M. P. McGovern, A. S. Reddy, N. L. Abbott, J. J. de Pablo, *Biochim. Biophys. Acta, Biomembr.* **2011**, *1808*, 26.

[19] J. W. M. Hoppener, B. Ahren, C. J. M. Lips, *N. Engl. J. Med.* **2000**, *343*, 411.

[20] R. P. R. Nanga, J. R. Brender, J. Xu, G. Veglia, A. Ramamoorthy, *Biochemistry* **2008**, *47*, 12689.

[21] R. H. Walters, R. M. Murphy, *J. Mol. Biol.* **2009**, *393*, 978.

[22] A. M. Woys, Y-S. Lin, A. S. Reddy, W. Xiong, J. J. de Pablo, J. L. Skinner, M. T. Zanni, *J. Am. Chem. Soc.* **2010**, *132*, 2832.

[23] M. D. De Tercero, N. L. Abbott, *Chem. Eng. Commun.* **2009**, *196*, 234.

[24] J. Buijs, W. Norde, J. W. T. Lichtenbelt, *Langmuir* **1996**, *12*, 1605.

[25] M. J. Swamy, T. Heimburg, D. Marsh, *Biophys. J.* **1996**, *71*, 840.

[26] C. Code, Y. Domanov, A. Jutila, P. K. J. Kinnunen, *Biophys. J.* **2008**, *95*, 215.

[27] I. Lascu, H. Porumb, T. Porumb, I. Abrudan, C. Tarmure, I. Petrescu, E. Presecan, I. Proinov, M. Telia, *J. Chromatogr.* **1984**, *283*, 199.

[28] R. Oldenbourg, *Live Cell Imaging: A Laboratory Manual* (Eds: R. D. Goldman, D. L. Spector), Cold Spring Harbor Laboratory Press, Cold Spring Harbor, NY **2005**, p. 205.

[29] a) V. Tomar, S. I. Hernandez, N. L. Abbott, J. P. Hernandez-Ortiz, J. J. de Pablo, *Soft Matter* **2012**, *8*, 8679; b) J. P. Hernandez-Ortiz, B. T. Gettelfinger, J. Moreno-Razo, J. J. de Pablo, *J. Chem. Phys.* **2011**, *134*, 134905; c) M. Rahimi, T. F. Roberts, J. C. Armas-Perez, X. Wang, E. Bukusoglu, N. L. Abbott, J. J. de Pablo, *Proc. Natl. Acad. Sci. USA* **2015**, *112*, 5297.

[30] a) C. W. Oseen, *Trans. Faraday Soc.* **1933**, *29*, 0883; b) F. C. Frank, *Discuss. Faraday Soc.* **1958**, *25*, 19.

[31] J. P. P. G. de Gennes, *The Physics of Liquid Crystals*, Oxford University Press Inc., New York **1995**.

[32] U. Kuhnau, A. G. Petrov, G. Klose, H. Schmiedel, *Phys. Rev. E* **1999**, *59*, 578.

[33] G. Barbero, R. Barberi, *J. Phys.* **1983**, *44*, 609.

[34] J. Linn, *Curr. Opin. Neurol.* **2014**, *27*, 380.

[35] F. Lavatelli, R. Albertini, A. Di Fonzo, G. Palladini, G. Merlini, *Clin. Chem. Lab. Med.* **2014**, *52*, 1517.

[36] N. Greenfie, G. D. Fasman, *Biochemistry* **1969**, *8*, 4108.